Hydrothermal synthesis, characterization and antimicrobial activity of Ag-modified ZnO nanoplates against pathogen

A. Ullah[a], A. M. Toufiq[a], M. T. Qureshi[b,*], A. Khan[a], M. Younas[c], S. T. Obeidat[b], M. Al Elaimi[b], R. A. Hameed[b], F. Ullah[a]
[a]*Department of Physics, Hazara University Mansehra, Mansehra, 21300, Pakistan*
[b]*Department of Basic Sciences, College of Preparatory Year, University of Ha'il, Ha'il 2440, Kingdom of Saudi Arabia*
[c]*Department of Microbiology, Government College University Faisalabad, Pakistan*

Antibiotic resistance is concerned with public health and a serious threat in modern world. Pathogenic strains are rapidly developing resistance against antibiotics and limiting the treatment options. Nanostructured zinc oxide (ZnO) shows significant results when doped with silver (Ag), therefore used as an antibacterial agent. In this work, we synthesized pure and varying concentration of Ag-doped ZnO nanoplates through a one-step hydrothermal route. The structural, morphological, and optical properties of prepared nanostructures were comparatively studied. Furthermore, we have performed the ager-well assay, minimum inhibitory concentration study, and minimum bactericidal concentration study of synthesized nanoplates against five different bacterial strains including *A. baumannii, P. aeruginosa, E. coli, K. pneumoniae,* and *S. aureus*. The antimicrobial screening shows that Ag-doped ZnO nanoplates are more effective against all pathogenic strains as compared to pure ZnO, and therefore can be used in biomedical science.

(Received April 17, 2022; Accepted 22, 2022)

Keywords: Hydrothermal synthesis, ZnO nanoplates, Antimicrobial activity, Minimum inhibitory concentration study

1. Introduction

In modern world, synthesizing various kind of novel hybrid metal oxide nanomaterials attracted great attention due to their sophisticated application in every field [1, 2]. On the other side, researchers are trying to overcome the resistance of the drug resistant pathogenic strains by using nanotechnology. *Staphylococcus aureus* (G-positive), *Escherichia coli*, *Acinetobacter baumannii*, *Pseudomonas aeruginosa, and Klebsiella pneumoniae* (G-negative) are the bacterial strains that have widely developed resistance against standard drugs and source of diversified spectrum of diseases [3]. In this regard, nanoparticle play an important role because it can be used as an alternative to organic drugs. Nanoparticles can interact and kill bacterial cells by destruction of protein, destruction of DNA through production oxygen reactive species (ROS), the release of cation, and by damaging peptidoglycan layer and cell membrane. When nanoparticles are exposed to radiation, they produce ROS that include O^-, H_2O_2, and OH^-. These peroxide and radicals play decisive role in the destruction of bacterial cell [3].

Zinc oxide (ZnO) is an environment friendly wide bandgap (3.40 eV) semiconductor. It has low threshold power and high exciton binding energy at room temperature. [4]. The nano-sized ZnO has a small diameter in the range of 10 - 100 nm and therefore is more dominant in the field of research and quasi-one-dimensional structure [5]. It can be used as electrode material for dye

* Corresponding author: tauseefqureshi1981@gmail.com
https://doi.org/10.15251/DJNB.2022.173.949

synthesized solar cell [6], gas sensor [7], transparent conductive coating [8], field emission material [9], electrical devices and as a antimicrobial agent [10].

Transition metals such as, Ni, Co, Mn, and Ag are used as dopants in ZnO to further enhance its properties for potential application in optical devices and novel memory storage. Doping is an effective way to tailor the optoelectronic properties and antibacterial activity of ZnO nanoparticles [11]. Now a days nano-sized drug particles are also used in pharmaceutical products [12]. The ZnO exhibit n-type semi conductivity due to natural defects such as oxygen vacancies, however, Ag-doping in zinc oxide is favorable to fabricate p-type ZnO. The Ag-doped ZnO is used in optoelectronic applications due to its high stability and compatibility with transparent and conducting oxide at high temperature [13]. Recently, it has been reported that zinc oxide nanoparticles could be used for food preservation as their toxicity and biosafety is evaluated [14]. When the Ag^+ ions are released by Ag-doped ZnO nanoparticles in aqueous solution, these ions have the ability to inhibit a large number of different pathogenic strains [15-17]. To saturate bandages, nanoparticles are used to resist the growth of bacteria on injury [18]. In our present study, we used a facile hydrothermal method for fabrication of bare and Ag-doped ZnO nanoplates. The structural and optical properties along with antibacterial activity for five different bacterial strains have been reported and discussed in detail.

2. Experimental

2.1. Materials and Method

Analytical grade Zn $(NO_3)_2.6H_2O$ (zinc nitrate hexahydrate), $AgNO_3$ (silver nitrate), KOH (potassium hydroxide) pallets, absolute ethanol, and de-ionized water were used to synthesize pure and Ag-doped ZnO. Nutrient agar and nutrient broth were used for antibacterial studies. A simple one-step hydrothermal route was used to synthesize pure and doped ZnO with different Ag concentration. The calculated amount i.e., 0.25 M zinc nitrate hexahydrate and 0.90 M potassium hydroxide solutions were mixed in de-ionized water. The potassium hydroxide solution was then poured drop wise in zinc nitrate hexahydrate solution under continuous stirring for 30 minutes. The homogenous solution was heated in a Teflon-lined Autoclave at 180 ºC for 18 hours. After the reaction was completed the Teflon-lined Autoclave was cool down to room temperature, white precipitates were settled down through centrifugation, washed three times with de-ionized water and absolute ethanol. After filtration the obtained precipitates were dried in oven at 120 ºC for 2 hours to obtain its powdered form.

2.2. Characterization

The crystalline purity of as-synthesized samples was investigated with Bruker X-ray diffractometer (AXS D8 Advance), field-emission scanning electron microscopy (Hitachi S-4700) was used to record morphological feature, chemical composition was evaluated through energy dispersive X-ray spectrometer (FEI Philips XL) and photoluminescence spectrum was obtained using photoluminescence spectrophotometer (Shimadzu UV-3150).

2.3. Antimicrobial study

The antimicrobial assay of the as-prepared nanoplates was performed against five different bacterial strains including *S. aureus* (G-positive), *A. baumannii*, *P. aeruginosa*, *E. coli*, and *K. pneumoniae* (G-negative) by using agar-well diffusion assay. These strains were clinical isolates and the antimicrobial tests were performed at the Department of Microbiology Government Collage University (GFCU) Faisalabad. All the equipment and glassware were sterilized, then molten agar media was poured on 5 petri dishes to prepare a uniform ~2-3 mm thick layer. Fresh bacterial culture was prepared by inoculating the nutrients broth for each experiment at 37 °C for 24 hours. The palates were then seeded with organism. Wells were bored with a sterile borer into ager-plates. Stock solution of $Zn_{1-x}Ag_xO$ (x=0 and 0.39) with a concentration 1-3 mg/ml was poured in wells. Inhibition zone were measured after incubation.

2.4. Minimum Inhibitory Concentration (MIC)

The MIC was performed by standard broth microdilution method recommended by Clinical Laboratory Standard Institute (CLSI) by using 96-well microtiter plate [19]. A twofold serial dilution of nanoplates and Mueller Hinton Broth (MHB) with a concentration range from 1000 μg/ml to 1.95 μg/ml was prepared and poured in wells. The microbial suspension with a $5x10^5$ cfu/ml was added into each well. The positive control (broth mixed with bacterial inoculum) and negative control (non-inoculum broth) was also maintained. The microtiter plate was then incubated at 37˚C for 24 hours. After incubation, the absorbance of the plat was recorded at wavelength of 600 nm through an Elisa plate reader. At the end, the nitro-blue tetrazolium chloride dye was added to visually confirmed the results.

2.5. Minimum Bactericidal Concentration

The MBC was determined by using Mueller Hinton Agar (MHA) plates. Suspension solution from the MIC wells was extracted and spread over ager plates, and incubated at 37 °C overnight. The plates were then examined for visual bacterial growth.

3. Results and Discussion

3.1. Structural Analysis

The XRD spectral analysis of pure and Ag-doped ZnO are presented in figure 1, recorded over the 2θ range of 10º-70º. The XRD peaks located at 2θ = 31.94, 34.66, 36.48, 47.75, 56.76, 63.03, 66.30, 68.19, and 69.35 are the reflection from (100), (002), (101), (102), (110), (103), (200), (112), and (201) planes. These peaks confirmed the formation of wurtzite hexagonal structure of ZnO, and are in agreement with the JCPDS reference card no # 36-1451. The doped samples show three additional peaks located at 2θ = 38.24, 44.32, and 64.39 of crystalline Ag along with the ZnO peaks. The intensity of crystalline Ag peaks is observed to increase with the dopant concentration while the intensity of ZnO peaks is decreased. The observed decrease in intensity is due to the incorporation of Ag^+ ions into ZnO lattice site, likely substituting Zn^{2+} ions. The lattice constant values of the hexagonal unit cell are calculated and tabulated in table 1. The high intensity of (101) peak suggest that growth of nanostructures has taken place essay direction of crystallization of ZnO [20]. The average grain size was estimated using the well-known Scherrer relation [21].

$$D = \frac{k\lambda}{\beta cos\theta} \quad (1)$$

where D is grain size, k = 0.94 is the Scherrer constant, λ is the wavelength of X-ray source, θ is Bragg's angle, and β is the FWHM. The calculated average grain size is in the range of 18.4 nm - 20.3 nm. It is observed that relatively smaller grain could be obtained for high concentration of Ag.

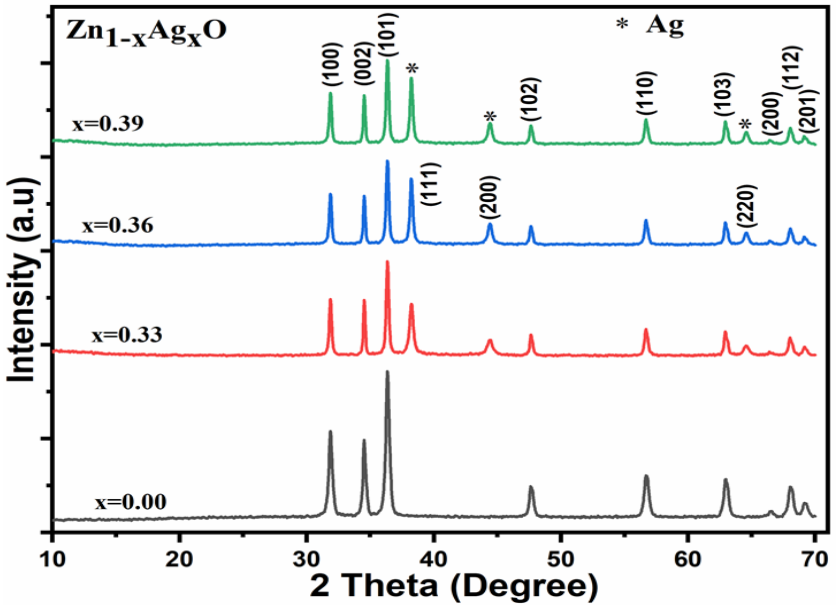

Fig. 1. XRD spectra of $Zn_{1-x}Ag_xO$ (x= 0.00, 0.33, 0.36 and 0.39) nanoplates.

Table 1. Unit cell lattice constant and average grain size of $Zn_{1-x}Ag_xO$ nanoplates.

Sample	Lattice parameters		Average grain size
$Zn_{1-x}Ag_xO$	a (Å)	c (Å)	D(nm)
x = 0.00	3.253	5.212	20.3
x = 0.33	3.249	5.205	19.2
x = 0.36	3.246	5.206	19.0
x = 0.39	3.247	5.210	18.4

3.2. Morphological and Elemental Composition studies

The morphological information of all prepared samples and their micrographs were obtained using field emission scanning electron microscopy as shown in figure 2. The images reveal the nanoplate-type morphology of the as-prepared nanostructures having an average diameter 235 nm, 175 nm, 159 nm and 143 nm for x = 0.00, 0.33, 0.36 and 0.39, respectively. Hence, by increasing the dopant concentration, the size of nanoplates decreases which is in agreement with the XRD analysis and no change in morphology was observed with the increase in dopant concentration. Furthermore, it can be observed that the nanoplates are evenly distributed for pure ZnO, but there is slight variation in size distribution for Ag-doped ZnO and due to this it appears as if distribution is densely or loosely packed [22].

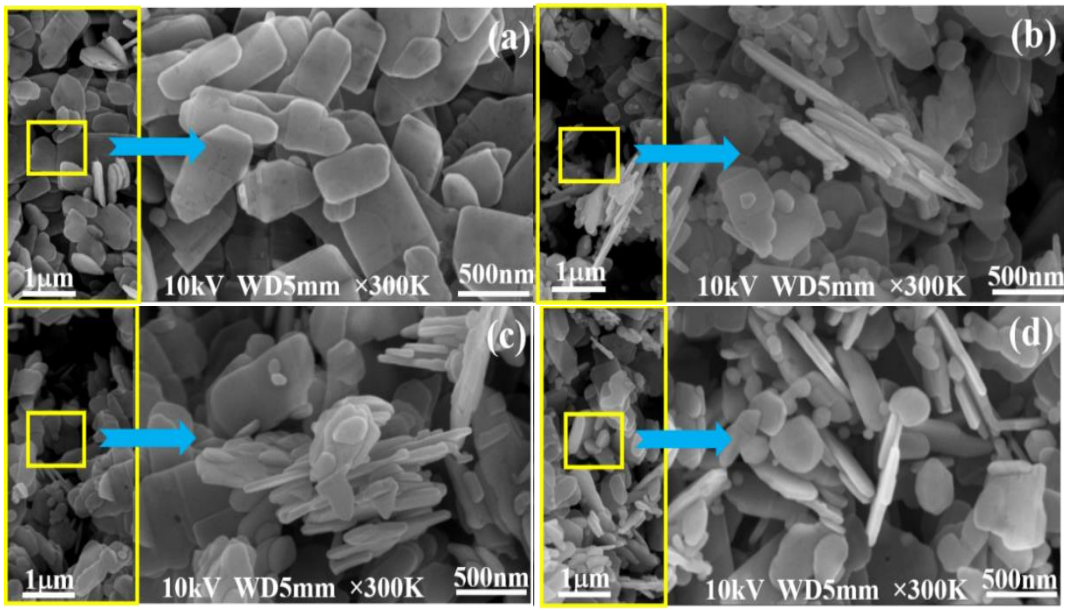

Fig. 2. Low- and high-resolution FESEM images of $Zn_{1-x}Ag_xO$ nanoplates (a) x= 0.00, (b) x= 0.33, (c) x= 0.36 and (d) x= 0.39.

Energy dispersive x-rays spectrum of as-prepared nanoplates was evaluated for their elemental confirmation as shown in figure 3. The presence of Zn, O, and Ag peaks confirms the formation of pure and Ag-doped ZnO. No other peaks related to impurity are observed which confirms the purity of as-prepared nanostructures.

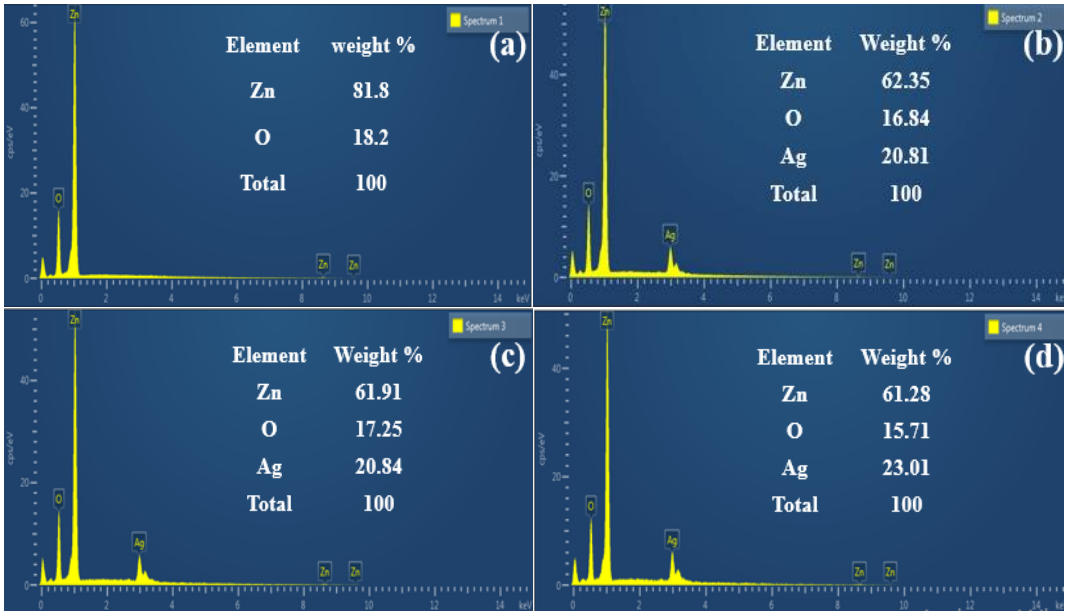

Fig. 3. EDX spectra of $Zn_{1-x}Ag_xO$ nanoplates (a) x= 0.00, (b) x= 0.33, (c) x= 0.36 and (d) x= 0.39.

3.3. Photoluminescence Studies

The photoluminescence (PL) emission spectra of synthesized nanoplates were recorded over the wavelength range of 350 - 800 nm. Figure 4 displays the obtained PL spectra of as-synthesized nanostructures having multiple emission bands in the ultraviolet and visible region. A

prominent intense and narrow PL emission peak recorded at 390 nm can be assigned to recombination of electron-hole pairs in valance and conduction band. The PL emission bands observed at 463 nm, 474 nm, 480 nm, and 484 nm are related to blue emissions due to the intrinsic and extrinsic defects. The intensity of emission band is observed to increase with the Ag content. The incorporation of Ag at substitutional sites causes reduction in electron-hole rate that can generate dual oxygen vacancies and active surfaces. This shows red shift and narrowing the bandgap region by pushing fermi-level towards valance band and enhancing photoluminescence property of ZnO [23].

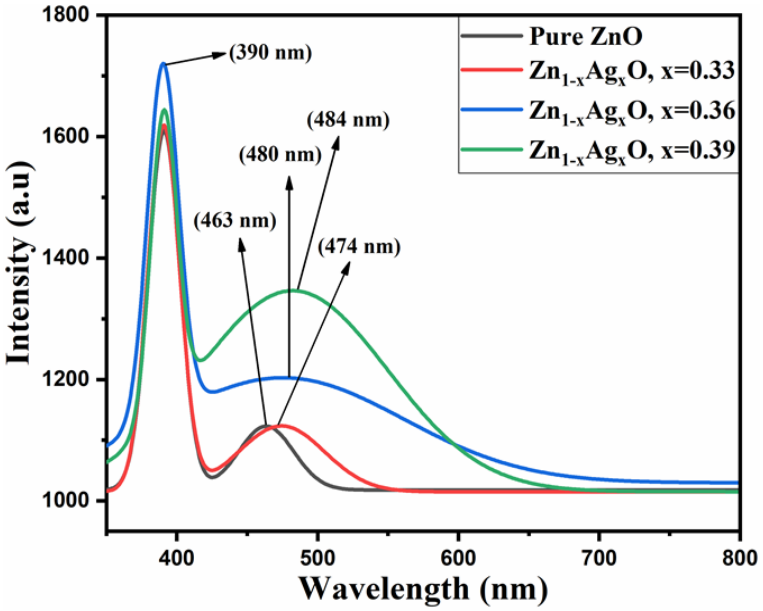

Fig. 4. Photoluminescence spectra of $Zn_{1-x}Ag_xO$ nanoplates (x= 0.00, 0.33, 0.36 and 0.39).

3.4. Optical Absorption Properties

The absorption spectra of the synthesized samples are recorded as a function of wavelength in the range of 200 - 800 nm and presented in figure 5 (a). The figure shows absorption band at 317 nm, 348 nm, 376 nm and 385 nm of the as prepared nanoplates. The absorption band for Ag-doped ZnO is shifted towards higher wavelength which causes a redshift in Ag-doped ZnO with decrease in energy bandgap [24]. The energy bandgap values of as-prepared nanostructures are calculated by Tauc relation [25].

$$(\alpha h\upsilon)^2 = k\,(h\upsilon - E_g) \quad (2)$$

Here *h* is planks constant, *k* is energy independent constant, α is absorption coefficient, υ is frequency of incident light and E_g is the bandgap energy. The $(\alpha h\upsilon)^2$ vs $h\upsilon$ plot is shown in figure 5 (b). The estimated bandgap energy is 3.33, 2.78, 2.61, and 2.50 eV for bare and Ag-doped ZnO.

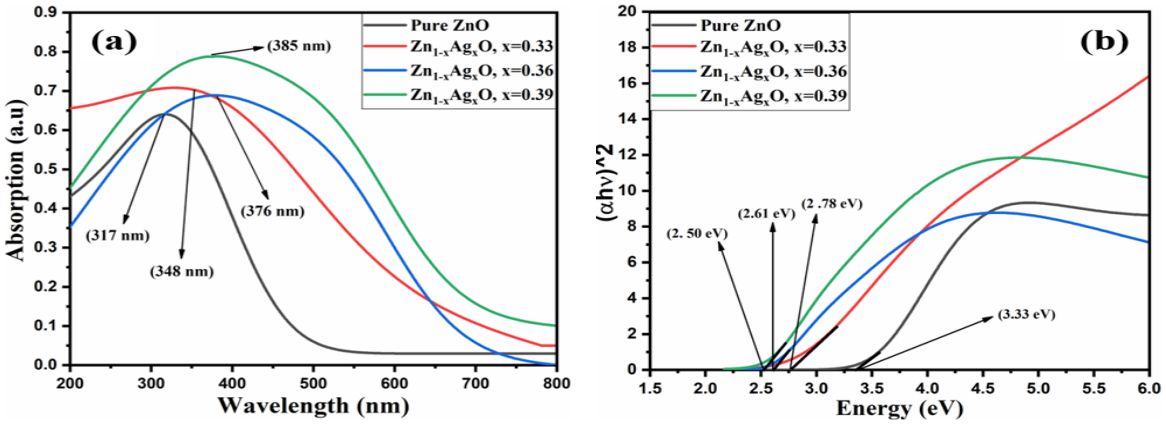

Fig. 5. (a) UV-visible absorption spectra, (b) Tauc Plot of $Zn_{1-x}Ag_xO$ (x= 0.00, 0.33, 0.36, 0.39) nanoplates.

3.5. Ager-well assay

The antimicrobial activity of the synthesized nanoplate is evaluated against five different clinical isolates including *A. baumannii*, *E. coli*, *S. aureus*, *P. aeruginosa*, and *K. pneumoniae* by using the agar well-diffusing assay. The antimicrobial tests for both (pure and Ag-doped ZnO) samples were performed at 3 different (1 mg, 2 mg, and 3 mg) nanoplates concentration as shown in figure 6. The diameter of inhibition zones was measured and tabulated in table 2. The ager-well result shows that Ag-doped ZnO is biologically more active as compare to pure ZnO. Shahid *et al.* [4] studied the antimicrobial sensitivity of pure and Ag-doped ZnO against different microbial strains and reported that Ag-doped ZnO exhibit better antimicrobial sensitivity as compare to pure ZnO. In present study, a maximum 18±0.73 mm diameter is observed at a concentration of 3 mg/ml for Ag-doped ZnO against *E. coli*. On contrary, the samples are less sensitive against *Staphylococcus aureus* that exhibit comparatively smaller zone of inhibition among all the strains. Nigussie *et al.* [26] reported that Ag-doped ZnO exhibit better antibacterial sensitivity against gram-positive as compare to gram-negative strains. In our study, the *Staphylococcus aureus* is the only gram-positive strain while the other are gram-negative. The gram-positive pathogens have much thicker cell wall as compare to gram-negative and therefore less sensitive against bioactive agent [27].

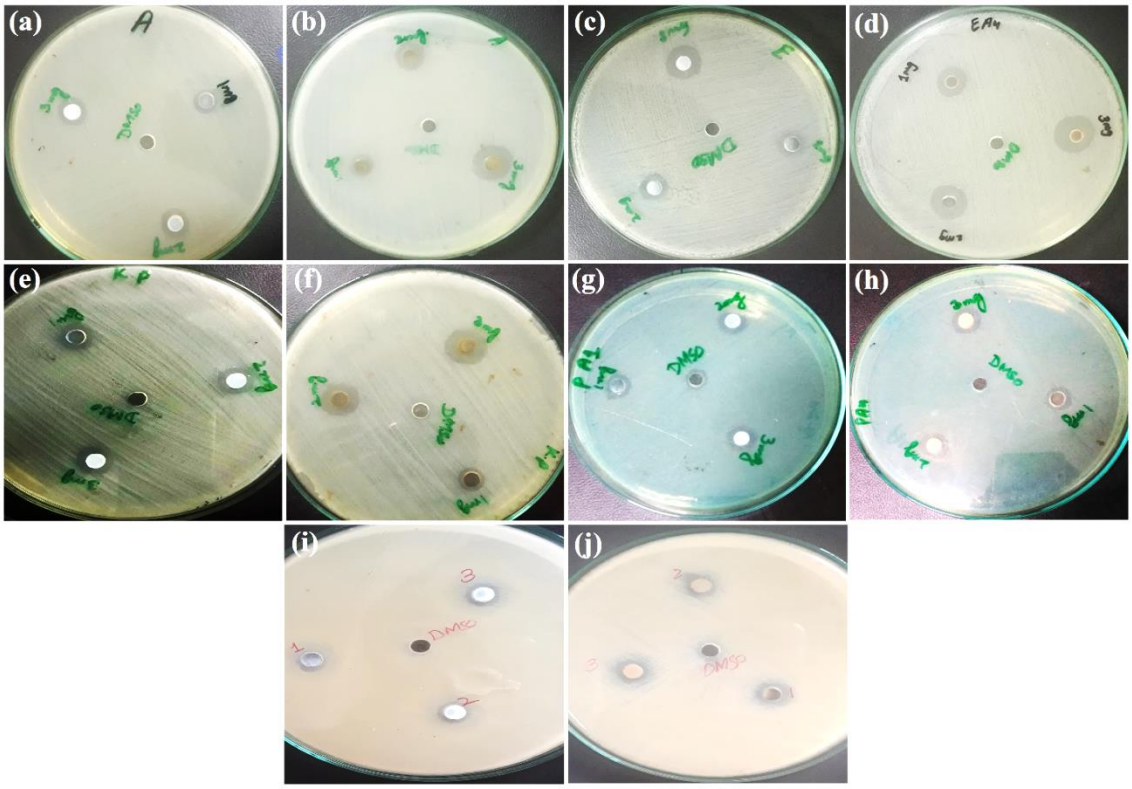

Fig. 6. Antibacterial activity of pure ZnO against (a) A. baumannii, (c) E. coli, (e) K. pneumoniae, (g) P. aeruginosa, (i) S. aureus. Antibacterial activity of Ag-doped ZnO against (b) A. baumannii, (d) E. coli, (f) K. pneumoniae, (h) P. aeruginosa, (j) S. aureus.

Table 2. Diameter of inhibition zone of pure and Ag-doped ZnO.

Bioactive agent		Inhibition zones (mm)				
		A. baumannii	*E. coli*	*K. pneumonia*	*P. aeruginosa*	*S. aureus*
ZnO	1 mg/ml	8 ±0.08	9±0.34	8±0.05	8±0.40	7.5±1.07
	2 mg/ml	9.5±0.79	10.5±0.87	8.5±0.75	9.5±0.22	8.5±0.46
	3 mg/ml	10±0.20	14±0.99	9±0.19	10.5±0.68	9±0.08
Ag/ZnO	1 mg/ml	8.5±0.32	10.5±0.51	7.5±0.38	8±0.07	10±0.11
	2 mg/ml	11±0.28	15±0.59	11±1.39	11 ±0.17	9±0.54
	3 mg/ml	15±1.03	18±0.73	13±0.97	12±0.28	11±0.92

3.6. Determination of Minimum Inhibition Concentration

The MIC is the lowest concentration of nanoplates at which there is no visible growth of bacteria. Figure 7 is the microtiter plate of MIC study and its corresponding data is tabulated in table 3. The result shows that MIC of nanoplates is effective at a dilution of 500 µg/ml. However, the MIC for *Escherichia coli* is observed to be 250 µg/ml for Ag-doped ZnO. Yousef *et al.* [28] studied MIC of ZnO against different pathogenic strains and reported that, *Escherichia coli* exhibit MIC at lower concentration as compare to other strains. Once nanoparticle is adsorbed on the surface of bacteria, it remains tightly bound with it even after the death of the cell. The bounded nanoparticles continue to release H_2O_2 into the medium and prevent bacterial growth [29].

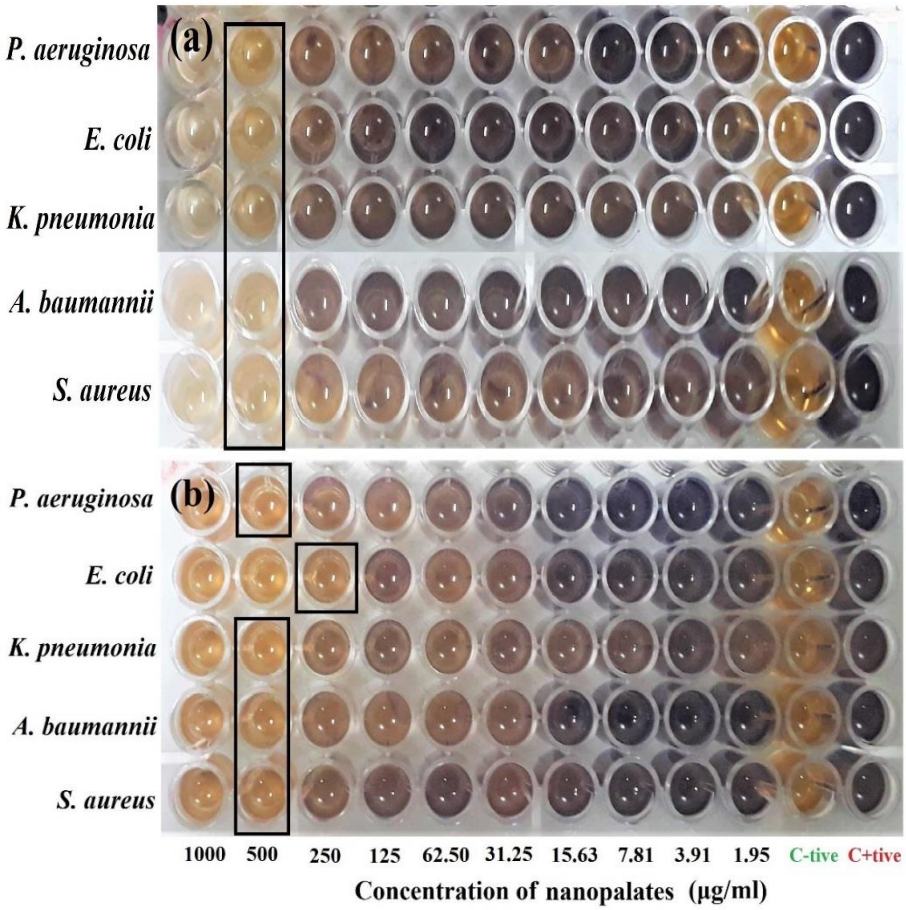

Fig. 7. Minimum inhibitory concentration (MIC) of (a) pure ZnO and (b) Ag-doped ZnO against S. aureus, P. aeruginosa, E. coli, A. baumannii and K. pneumoniae.

Table 3. The "+" sign represent growth while the "-" sign no growth of the microtiter plate of S. aureus, P. aeruginosa, E. coli, A. baumannii, and K. pneumoniae.

Strain	Concentration of pure ZnO (µg/ml)									
	1.95	3.91	7.81	15.63	31.25	62.50	125	250	500	1000
A. baumannii	+	+	+	+	+	+	+	+	*MIC/MBC*	-
E. coli	+	+	+	+	+	+	+	+	*MIC/MBC*	-
K. pneumonia	+	+	+	+	+	+	+	+	*MIC*	*MBC*
P. aeruginosa	+	+	+	+	+	+	+	+	*MIC*	*MBC*
S. aureus	+	+	+	+	+	+	+	+	*MIC*	*MBC*
Concentration of Ag-doped ZnO (µg/ml)										
A. baumannii	+	+	+	+	+	+	+	+	*MIC/MBC*	-
E. coli	+	+	+	+	+	+	+	*MIC*	*MBC*	-
K. pneumonia	+	+	+	+	+	+	+	+	*MIC*	*MBC*
P. aeruginosa	+	+	+	+	+	+	+	+	*MIC/MBC*	-
S. aureus	+	+	+	+	+	+	+	+	*MIC*	*MBC*

3.7. Determination of Minimum bactericidal concentration

The MBC study of the two wells of microtiter plate was performed by using the MHA plates. The visible bacterial growth is enclosed in a red ellipse as shown in figure 8. Figure 8a-d shows that the MBC of pure ZnO against *A. baumannii* and *E. coli* occurred at the same

concentration as the MIC (500 µg/ml). However, for *K. pneumoniae*, *S. aureus*, and *P. aeruginosa* (figure 8e-j) it is observed at a higher concentration (1000 µg/ml). On the other hand, the MBC of Ag-doped ZnO against *A. baumannii, E. coli*, and *P. aeruginosa* occurred at 500 µg/ml, while for *K. pneumoniae* and *S. aureus at* 1000 µg/ml (figure 8k-t). In the present study, the antimicrobial results suggests that Ag-doped ZnO nanoplates exhibit relatively better performance as compare to pure ZnO, therefore it could be used as an efficient antimicrobial agent.

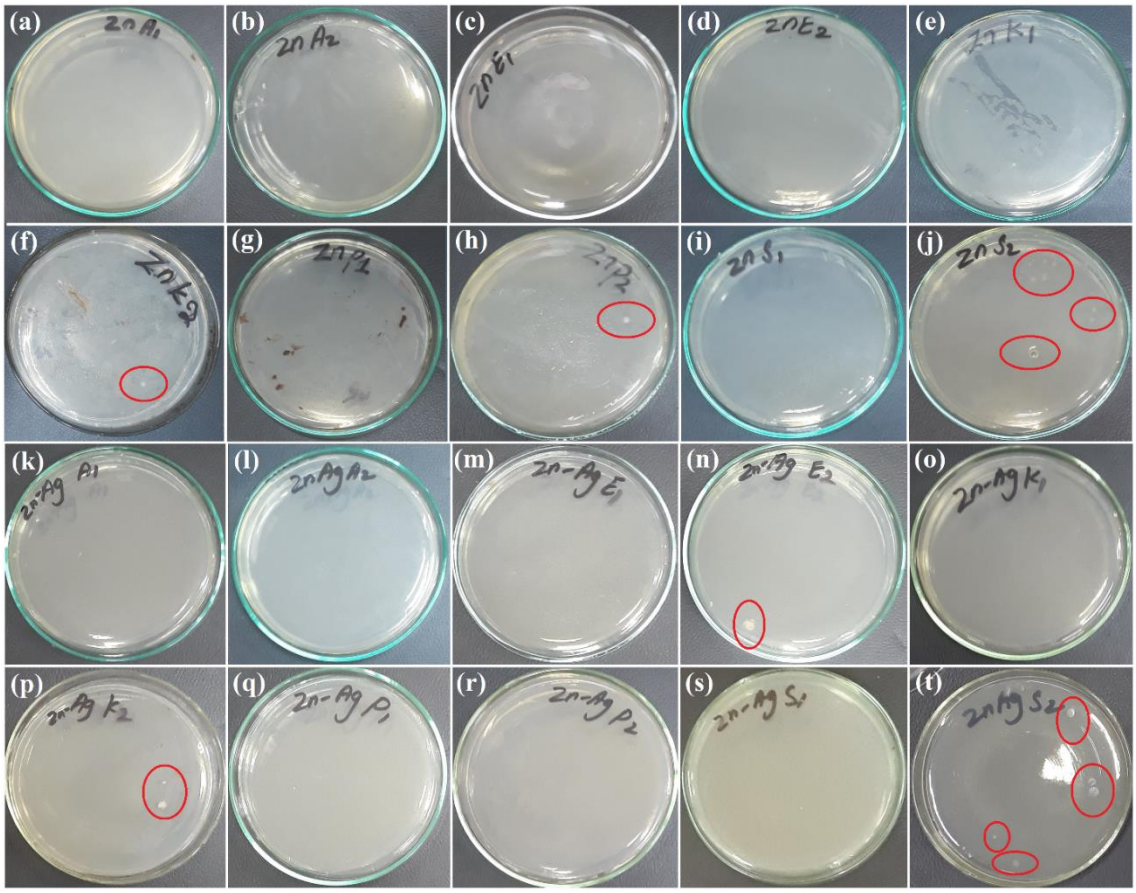

Fig. 8. Mueller Hinton Agar (MHA) plates of minimum bactericidal concentration (MBC) of pure ZnO for (a-b) A. baumannii, (c-d) E. coli, (e-f) K. pneumoniae, (g-h) P. aeruginosa, and (i-j) S. aureus. MHA plates of MBC of Ag-doped ZnO (k-l) A. baumannii, (m-n) E. coli, (o-p) K. pneumoniae, (q-r) P. aeruginosa, and (s-t) S. aureus.

4. Conclusion

Pure and Ag-doped ZnO nanoplates were synthesized through a facile hydrothermal route. The synthesized nanoplates were characterized by XRD, SEM, EDX, PL, UV-vis absorption spectroscopy, and their antibacterial activity was evaluated against *A. baumannii, E. coli, P. aeruginosa, K. pneumoniae*, and *S. aureus* strains for their efficiency. The XRD pattern showed the hexagonal wurtzite structure without any impurities. The FESEM revealed nanoplates morphology of the as-prepared samples. The EDX analysis confirmed that the pure sample is composed of Zn and O while the doped samples additionally contain Ag atoms. The photoluminescence spectra showed emissions bands in the ultraviolet and visible regions of the electromagnetic spectrum. Furthermore, the ultraviolet-visible absorption studies showed a redshift in the bandgap energy with the increasing concentration of Ag. The antibacterial results revealed that Ag-doped ZnO is more effective against tested bacterial strains as compared to pure ZnO. We

believe that the synthesized ZnO nanoplates could have potential use in pharmaceutics and have a valuable scope of advanced research in areas of sterile coatings and wound dressings.

Acknowledgments

This research has been funded by Scientific Research Deanship at University of Ha'il-Saudi Arabia through project number RG-21 063.

References

[1] X. Deng, L. Zhang, J. Guo, Q. Chen, J. Ma, Material Research Bulletin 90 170-174 (2017); https://doi.org/10.1016/j.materresbull.2017.02.040

[2] S. Lee, Y. Park, D. Kim, D. Baek, J. Yi, B. Hong, W. Choi, J. Lee, Material Research Bulletin 58, 126-131(2017); https://doi.org/10.1016/j.materresbull.2014.04.050

[3] A. Khan, R. Hussain, A. M. Toufiq, A. Shah, B.A. Khan, Z. Niaz, S. ur Rahman, Materials Characterazation 169, 110661 (2020); https://doi.org/10.1016/j.matchar.2020.110661

[4] S. Shahid, S. Khan, W. Ahmad, U. Fatima, S. Knawal, Indian Journal of Pharmaceutical Sciences, 80(1), 173-180 (2018); https://doi.org/10.4172/pharmaceutical-sciences.1000342

[5] I. Sondi, B. Salopek-Sondi, Journal of colloid and interface science, 275(1), 177-182 (2004); https://doi.org/10.1016/j.jcis.2004.02.012

[6] A. Qurashi, M. Hossain, M. Faiz, N. Tabet, M.W. Alam, N.K. Reddy, rnal of Alloys andJou Compound 503(2), L40-L43 (2010); https://doi.org/10.1016/j.jallcom.2010.05.022

[7] Q. Ahsanulhaq, J. Kim, J. Lee, Y. Hahn, Electrochemistry Communications, 12(3), 475-478 (2010); https://doi.org/10.1016/j.elecom.2010.01.023

[8] T. Minami, Journal of Vacuum Science & Technology A: Vacuum, Surfaces, and Films, 17(4), 1765-1772 (1999); https://doi.org/10.1116/1.581888

[9] F. Jamali-Sheini, R. Yousefi, M.A. More, D.S. Joag, Materials Letters 111, 181-184 (2013); https://doi.org/10.1016/j.matlet.2013.08.073

[10] J. Pivin, G. Socol, I. Mihailescu, P. Berthet, F. Singh, M. Patel, L. Vincent, Thin Solid Films, 517(2), 916-922 (2008); https://doi.org/10.1016/j.tsf.2008.08.125

[11] A. Shah, M.B. Ahamed, E. Manikandan, R. Chandramohan, M. Iydroose, Journal of Materials Science: Materials in Electronics, 24(7), 2302-2308 (2013); https://doi.org/10.1007/s10854-013-1093-6

[12] Y. K. Jo, B.H. Kim, G. Jung, Plant disease, 93(10), 1037-1043 (2009); https://doi.org/10.1094/PDIS-93-10-1037

[13] T. Herng, S.P. Lau, S.F. Yu, H. Yang, L. Wang, M. Tanemura, J. Chen, Applied Physics Letters 90(3), 032509 (2007); https://doi.org/10.1063/1.2433028

[14] S. Siddique, Z. Hussain, S. Shahid, F. Yasmin, Preparation, characterization and antibacterial activity of ZnO nanoparticles on broad spectrum of microorganisms, (2013).

[15] M. Kawashita, S. Tsuneyama, F. Miyaji, T. Kokubo, H. Kozuka, K. Yamamoto, Biomaterials, 21(4), 393-398 (2000); https://doi.org/10.1016/S0142-9612(99)00201-X

[16] W. C. Lin, C.-N. Chen, T. T. Tseng, M.-H. Wei, J. Hsieh, W.J. Tseng, Journal of the European Ceramic Society, 30(14), 2849-2857 (2010); https://doi.org/10.1016/j.jeurceramsoc.2009.12.016

[17] S. Pal, Y. K. Tak, J. M. Song, Applied and environmental microbiology, 73(6), 1712-1720 (2007); https://doi.org/10.1128/AEM.02218-06

[18] M. Kassaee, A. Akhavan, N. Sheikh, A. Sodagar, Journal of applied polymer science, 110(3), 1699-1703 (2008); https://doi.org/10.1002/app.28762

[19] R. Miller, R. Walker, J. Carson, M. Coles, R. Coyne, I. Dalsgaard, C. Gieseker, H. Hsu, J. Mathers, M. Papapetropoulou, Diseases of aquatic organisms, 64(3), 211-222 (2005);

https://doi.org/10.3354/dao064211
[20] H.-F. Lin, S.-C. Liao, S.-W. Hung, Journal of photochemistry and photobiology A: Chemistry, 174(1), 82-87 (2005); https://doi.org/10.1016/j.jphotochem.2005.02.015
[21] N. Ullah, M. T. Qureshi, A. M. Toufiq, F. Ullah, M. Al Elaimi, R. S. A. Hameed, A. Khan, H.M.E. Ragab, Applied Physics A, 127(10), 1-7 (2021); https://doi.org/10.1007/s00339-021-04926-7
[22] C. Abinaya, M. Marikkannan, M. Manikandan, J. Mayandi, P. Suresh, V. Shanmugaiah, C. Ekstrum, J. M. Pearce, Materials Chemistry and Physics, 184 (2016) 172-182; https://doi.org/10.1016/j.matchemphys.2016.09.039
[23] I. Ahmad, E. Ahmed, M. Ullah, A. Rana, M. Manzoor, M. Rasheed, A. Malik, N. Khalid, M. Ahmad, U. Mehtab, Journal of Ovonic Research, 14 (2018).
[24] E. Burstein, Physical Review 93(3), (1954) 632; https://doi.org/10.1103/PhysRev.93.632
[25] A. Khan, A. M. Toufiq, F. Tariq, Y. Khan, R. Hussain, N. Akhtar, S. ur Rahman, Materials Research Express, 6(6), 065043 (2019); https://doi.org/10.1088/2053-1591/ab0aaf
[26] G. Y. Nigussie, G. M. Tesfamariam, B. M. Tegegne, Y. A. Weldemichel, T. W. Gebreab, D. G. Gebrehiwot, G. E. Gebremichel, International Journal of Photoenergy, 2018 (2018); https://doi.org/10.1155/2018/5927485
[27] O. Sizar, C. G. Unakal, Gram positive bacteria, StatPearls [Internet], (2020).
[28] J. M. Yousef, E. N. Danial, Journal of Health Science 2(4), 38-42 (2012); https://doi.org/10.5923/j.health.20120204.04
[29] N. Padmavathy, R. Vijayaraghavan, Science and technology of advanced materials, (2008); https://doi.org/10.1088/1468-6996/9/3/035004